Journal of Materials Chemistry C

Accepted Manuscript

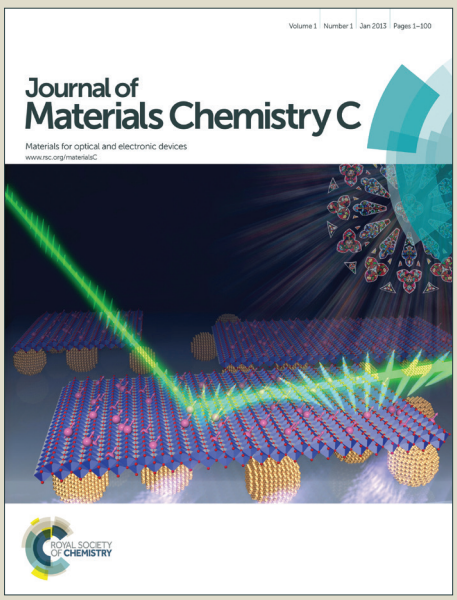

This is an *Accepted Manuscript*, which has been through the Royal Society of Chemistry peer review process and has been accepted for publication.

Accepted Manuscripts are published online shortly after acceptance, before technical editing, formatting and proof reading. Using this free service, authors can make their results available to the community, in citable form, before we publish the edited article. We will replace this *Accepted Manuscript* with the edited and formatted *Advance Article* as soon as it is available.

You can find more information about *Accepted Manuscripts* in the Information for Authors.

Please note that technical editing may introduce minor changes to the text and/or graphics, which may alter content. The journal's standard Terms & Conditions and the Ethical guidelines still apply. In no event shall the Royal Society of Chemistry be held responsible for any errors or omissions in this *Accepted Manuscript* or any consequences arising from the use of any information it contains.

ROYAL SOCIETY OF CHEMISTRY

www.rsc.org/materialsC

Single Molecule Magnets Grafted on Gold: Magnetic Properties From Ab Initio Molecular Dynamics†

Alessandro Lunghi[a], **Marcella Iannuzzi**[b], **Roberta Sessoli**[a] **and Federico Totti**[*a]

Received Xth XXXXXXXXXX 20XX, Accepted Xth XXXXXXXXX 20XX
First published on the web Xth XXXXXXXXXX 200X
DOI: 10.1039/b000000x

A computational characterization of the Single Molecule Magnet (SMM) [Fe_4(AcS $(CH_2)_5C(CH_2O)_3)_2$(dpm)$_6$] (Fe_4C_5) with Ac = CH_3CO and Hdpm = dipivaloylmethane, grafted on Au(111) surface (Fe_4C_5@Au(111)) is presented. For the first time Ab initio Molecular Dynamics (AIMD) calculations have been used to study the evolution of the structural properties of a SMM once adsorbed on a metallic substrate. Important structural rearrangements induced by the grafting process can be observed thanks to the AIMD approach. This allows to elucidate some possible mechanisms that govern the SMM's magnetism on surface, which wouldn't be revealed by the standar static approach. The sampling of the SMM@Au(111)'s configurational space at finite temperature, together with magneto-structural correlations, makes it possible to study the fluctuation amplitude of magnetic properties, thus revealing that a single minimum of the free energy surface (FES) is populated at 200 K. Starting from the finite temperature scenario, the potential energy surface (PES) was sampled by means of thermal annealing calculations showing that multiple local minima could be populated at 0 K. Both isotropic exchange coupling constants and zero field splitting (ZFS) parameters are calculated for the identified Fe_4C_5@Au(111) local minima, thereby allowing an in-depth characterization of the Fe_4C_5 magnetic properties from the isolated to the grafted scenario. The cutting-edge computational protocol used here shows that the experimentally observed retention of a spin $S = 5$ ground state upon grafting results from balancing the major modifications on spin Hamiltonian (SH) parameters. Electronic effects of the metal on Fe_4C_5's magnetic properties have been also discussed.

1 Introduction

The possibility to employ just few atoms to observe magnetic bistability, and thus retain information, has been recently demonstrated,[1,2] opening new frontiers in the high-density data storaging with a potential increase of orders of magnitude with respect to capabilities available in nowadays magnetic data supports. In order to reach such great technological performances a system able to show an intrinsic magnetic hysteresis loop coming from its intramolecular properties is needed. In this context Single Molecule Magnets (SMMs) represent one of the best candidates to be used for magnetic data recording and in spintronic devices in general, though up to now only at cryogenic temperature.[3,4] Their peculiar magnetic properties have been intensively studied as far as from the first observation of their molecular hysteresis loop[5] and still, after almost twenty years, the interest on this class of molecular compounds has not diminished yet. However, in order to be integrated into real devices, SMMs must show enough robustness upon grafting or absorption process on surfaces.

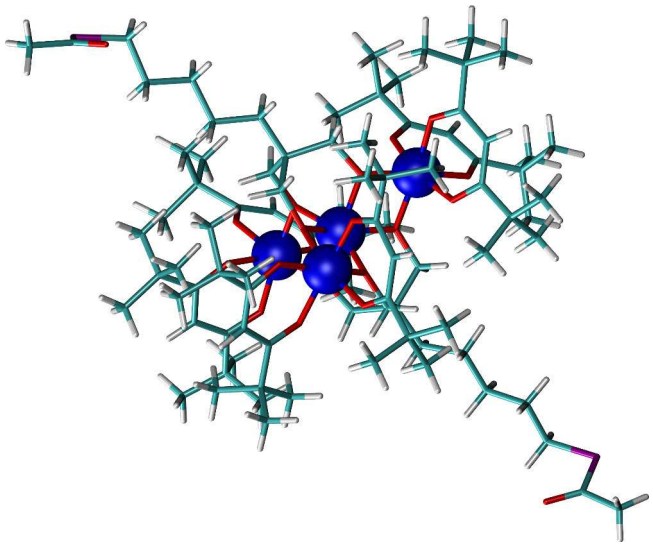

Fig. 1 Sketch of Fe_4C_5 molecule. Iron atoms are colored in blue, oxygen atoms in red, sulfur atoms in purple, carbon atoms in green and hydrogen atoms in white.

The SMM studied in this work, the propeller-shaped Fe_4C_5[6] (see Fig. 1), showed to be robust enough to retain its magnetic hysteresis loop[7] once grafted on Au(111). There-

† Electronic Supplementary Information (ESI) available. See DOI: 10.1039/b000000x/

[a] *Universitá degli Studi di Firenze. Dipartimento di Chimica "Ugo Schiff", Via della Lastruccia 3-13, 50019, Sesto Fiorentino (FI); E-mail: federico.totti@unifi.it*
[b] *Institute of Physical Chemistry, University of Zurich, Winterthurerstrasse 190, CH-8057 Zurich, Switzerland*

Journal of Materials Chemistry C Accepted Manuscript

fore, it is an appealing candidate for throughout analysis on how the magnetic properties change upon deposition on a surface. Fe_4C_5, in its crystalline environment, has an $S = 5$ ground state which originates from the leading antiferromagnetic coupling between the central high spin Fe^{3+} ion (Fe_c or Fe_1) and the three peripheral high spin Fe^{3+} ions (Fe_p or Fe_2, Fe_3 and Fe_4). Although experimental data are usually interpreted assuming a threefold symmetry, the Fe_4C_5 has only a two-fold symmetry passing through the Fe_1-Fe_2 direction. However, in order to account for the effects on the magnetic properties caused by possible geometrical deviations from the crystalline symmetry, the Hamiltonian describing isotropic interactions is written as

$$H = J_{12}\vec{s}_1 \cdot \vec{s}_2 + J_{13}\vec{s}_1 \cdot \vec{s}_3 + J_{14}\vec{s}_1 \cdot \vec{s}_4 + J_2\left(\vec{s}_2 \cdot \vec{s}_3 + \vec{s}_2 \cdot \vec{s}_4 + \vec{s}_3 \cdot \vec{s}_4\right). \quad (1)$$

Here, J_{1x} (x = 2-4) are the first and J_2 the second neighbor exchange interactions (J_2 is left three-fold since it is usually below 1 cm^{-1}). The magnetic memory effect, *i.e.*, the opening of magnetic hysteresis loop, is originated by the degeneracy lifting of the ground state multiplet due to the anisotropy term of the spin Hamiltonian,

$$H = \sum_i \vec{s}_i \cdot \mathbf{D_i} \cdot \vec{s}_i + \sum_{i,j \neq i} \vec{s}_i \cdot \mathbf{D_{ij}} \cdot \vec{s}_j. \quad (2)$$

In the above expression, i and j run over the spin ($\vec{s}$) of the four iron ions. Alternatively, in the Giant Spin approximation (GSA), the same anisotropic physical behavior could be modeled as

$$H = \vec{S} \cdot \mathbf{D}_{S=5} \cdot \vec{S}, \quad (3)$$

where $\vec{S}$ now stands for the ground state giant spin $S = 5$ vector.

A detailed experimental characterization of Fe_4C_5@Au(111) can be achieved only through an interplay between different techniques.[8] In particular, the difficult access to accurate structural information poses major limitations onto the full understanding of deposited SMMs properties. Indeed, the absence of an atomically resolved structure makes the assessments of the origin of the observed magnetic phenomena difficult to be unambiguously rationalized. In this scenario a cutting-edge theoretical description of SMMs deposited on surfaces becomes mandatory to fill up the missing information and therefore to draw a final picture of the SMM@Au(111) system. In this framework, we present here a complete and detailed DFT computational description of the structural and magnetic properties of Fe_4C_5@Au(111) employing both static and dynamic approaches. X-ray derived geometries are commonly used for the calculation of magnetic properties of SMMs. In some studies, to account for the effects of adsorption on surfaces, the structures have been optimized at the level of theory of choice.[9–11] However, static optimization approaches are not adequate to describe a complex configurational space that could present multiple minima, as it is expected to be the case by deposition of SMMs on surfaces. On the other hand, ab initio molecular dynamics (AIMD) provides a proper sampling of the accessible space of configurations at finite temperature. The generated trajectory is expected to visit the accessible structures according to their statistical probability at the selected thermodynamic conditions. In this respect, the MD simulation samples the free energy surface (FES) underlying the dynamic of the system of interest, and reproduces its characteristic thermal fluctuations. Recently AIMD has been applied to the study of Spin crossover magnetic systems containing Fe^{2+} ions.[12,13] However, at the best of our knowledge, this computational strategy has never been applied before to study hybrid systems (adsorbate@surface) containing hundreds of heavy atoms and with a complex magnetic structure as the one observed for SMMs. Indeed, a similar statistical analysis restricted to only isotropic magnetic properties has been previously computed only at the QM/MM level for a metalloprotein system[14] containing two iron ions bridged by di-sulfuric bridge as catalytic center. The AIMD application to the study of the grafting process of Fe_4C_5@Au(111) will be reported in the first part of this work where we obtained both dynamical information and steady state structures which could well statistically describe the molecular geometry once the SMM is grafted on Au(111). The so computed accurate atomistic picture of the system is of fundamental importance in order to understand how the deposition on a metallic surface affects the molecular magnetic properties. In the second part of the work, a comprehensive magnetic characterization of the computed geometries will be presented within the framework of previous successfully tested computational protocols[9,15–17] based on GGA, GGA+U and hybrid functionals.

2 Computational Strategy and Methods

When a trend of physical properties must be evinced, it is of fundamental importance to handle all the elements of the ensemble with the same computational procedure. Such a care must be used in order to enforce the homogeneity of the results and reduce the source of errors coming from unbalanced computational treatments. Since the geometry of grafted species can not be determined at the experimental level (it can only be qualitatively extrapolated in simple cases, *i.e.*, adsorbed porphyrins[18]), the calculation of the relaxed geometry, through structure optimization, of the SMM on the surface becomes mandatory. Therefore, in order to study the evolution of the magnetic properties from the bulk to the grafted scenario, the same optimization procedure must be applied also to the SMM bulk phase. The magnetic data computed on optimized geometries become the reference values to compare to those computed in the grafted scenario. In order to have comparable magnetic properties, each spin Hamiltonian parameter must be computed with the same electronic structure approach before and after the grafting. The choice of the computational

Journal of Materials Chemistry C Accepted Manuscript

protocol clearly depends on the properties we are interested in. GGA DFT calculations are known to accurately determine optimized structures of large systems. However, the accurate calculation of magnetic properties, *e.g.* the calculation of exchange coupling parameters, may require the use of hybrid functionals. The mixed computational protocol proposed in this work allows us to determine the evolution of the SMM's magnetic properties from bulk to the grafted scenario. The reference bulk structure optimization and the AIMD simulations have been carried out with the TPSS functional[19] corrected for the dispersion forces using the Grimme's formalism[20]. The calculation of exchange coupling parameters would require the use of hybrid functionals, while the anisotropic part of the spin Hamiltonian could be accurately calculated with the less demanding PBE functional. However, applying hybrid functionals to large periodic systems (SMM bulk and grafted on a surface) and over many configurations becomes computationally unaffordable. For this reason, the isotropic exchange coupling constants have have been calculated at the PBE+U level of theory.[21] PBE0 calculations have been carried out for isolated systems and compared to the PBE+U results, in order to asses the reliability of the parametric Hubbard correction (see Methods for further details).

2.1 Models

The Au(111) surface has been modeled as a four layers slab of gold. Each layer consists of 80 gold atoms. The dimensions of the simulation cell are 23.05 x 25.0 x 60.0 Å. Periodic boundary conditions are always applied, but the size of the box is sufficient to avoid interactions between periodic images of the Fe_4C_5 units, which are about 10 Å apart from each other. From experimental and computational evidances it can be assessed that both thioacetyl and simple thiols undergo an homolithyc cleavage of the S-Ac (S-H) bond with the formation of a sulfur radical, which is the species that effectively binds the metallic substrate.[22,23] The Fe_4C_5 molecule has two side chains, each containing one thioacetyl group. Thanks to the steric hindrance of the magnetic core, only one of the two chains can actually bind to the substrate[24]. According to literature[22,23,25,26], the initial configuration was prepared grafting the X-ray structure of Fe_4C_5 upon the Au(111) after the removal of one Ac· group from one aliphatic chain, while leaving intact the other one.

2.2 AIMD and optimizations

AIMD calculations within the Born-Oppenheimer framework have been performed optimizing the wave function at each MD step. Electronic structure and nuclear forces have been calculated at the meta-GGA DFT level of theory, applying the Gaussian and plane wave (GPW) method[27,28], as implemented in CP2K[29]. The GPW approach is based on the expansion of the valence electron molecular orbitals in Gaussian type orbital basis sets, for which we use molecule optimized basis sets of the DZVP-MOLOPT-SR-GTH type.[30] The auxiliary plane wave basis set is needed for the representation of the electronic density in the reciprocal space and the efficient solution of the Poisson's equation. We truncate the plane wave basis set at 400 Ry. The interactions between valence electrons and atomic cores are described by means of Godecker-Teter-Hutter pseudopotentials.[31,32] In particular, we used the TPSS[19] functional together with the Grimme's D3 corrections[20] to account for the dispersion forces. The computational set up has been tested on bulk Au, Au(111) surface energy and cohesive energy of Benzene on Au(111) (available on ESI). The selected set up can adequately reproduce the structure of both gold slab and grafted molecule.

Hamiltonian equations of motion are numerically integrated using the velocity Verlet algorithm and a time step of 1 fs. Canonical distribution of momenta at 200 K is enforced with the canonical stocastic rescaled velocity (CSVR) thermostat[33] with a time constant of 100 fs during thermalization and 500 fs during acquisition runs. Independent trajectories starting from the same initial configuration are generated by first initializing the velocities at 100 K and then annealing the system up to 200 K by different ramp procedures. Total energy conservation has been obtained with a smearing of molecular orbitals' occupation numbers with a Fermi-Dirac distribution at 1500 K and with a convergence threshold criteria on the maximum wave function's gradient of 1.0E-5.

When dealing with multispin systems, the DFT solution which can be used to evaluate forces is not unequivocally defined. Various spin solutions, described by broken symmetry (BS) states, are available. For what concern the overall structure of the complex and its interaction with the surface, the choices of one spin DFT solution instead of another is not important and no appreciable differences should be expected. For this reason, all the AIMD calculations are carried out with forces evaluated from the electronic configuration that better describes the lowest energy spin multiplet ($S = 5$): the central iron (Fe_c or Fe_1) is down polarized while the peripheral irons (Fe_p or Fe_{2-4}) are up polarized (schematically DUUU).

2.3 Magnetic Properties Calculations

Magnetic properties analysis have been carried out utilizing both CP2K and ORCA software. For what concerns the extrapolated geometries we used the procedure recently tested over a series of different Fe_4 SMMs[15]. This procedure consists in two steps. The first one requires the CP2K code with the hybrid PBE0 functional[34] for the calculation of the isotropic exchange coupling constants. The PW cutoff have been set to 400 Ry, DZVP-MOLOPT-SR basis sets with GTH pseudo potentials have been chosen for all the elements. For the evaluation of exact exchange integrals we take advantage of an auxiliary basis set[35]: the DZVP-MOLOPT-SR basis set has been used for iron ions while the SZV-MOLOPT-SR basis set was chosen for carbon, hydrogen, oxygen and sulfur

Journal of Materials Chemistry C Accepted Manuscript

atoms. Convergence criteria over the maximum component of the wavefunction's gradient were set to 1.0E-6. Following the Noodleman formulation of the BS approach[36,37], isotropic exchange coupling constants have been extracted solving the linear system

$$\Delta E\left(HS - BS(\{s_k\})\right) = \sum_{ij} 2J_{ij}s_i s_j \lambda_{ij}^{BS} \quad (4)$$

where s_i and s_j are the value of the single ion spins, J_{ij} their exchange interaction and λ_{ij} is equal to one if, for the specific BS state considered with the appropriate s_k value, the couple of spin (i,j) are misaligned, zero otherwise. The SH considered to model the multiplet structure of the Fe_4C_5 is given in Equation 1. In order to solve the system 4 for the SH model 1 we used four different energy differences built up by the HS state and the four BS determinants: DUUU, UDUU, UUDU and UUUD. Once the non relativistic multiplets structure is obtained, it is then possible to proceed with the second step, where the calculation of the anisotropy tensors is performed. For this second task the software ORCA has been utilized. The computationally cheap GGA (PBE) functional has been used, since the expensive PBE0 is found not to improve the results.[15] We used the def2-TZVP basis set for all the elements and the RI approximation for the coulomb operator integral evaluation have been employed with the def2-TZVP/J auxiliary basis set. Speaking in the ORCA notation, Grid 5 and Very Tight convergence criteria were used. The protocol used to compute anisotropy splittings follows the route of the diamagnetic substitution. We evaluated single ion tensors making the substitution of all but one iron ions with Ga^{3+} ions at turn. Both Spin Orbit Coupling (SOC) and Spin Spin (SS) interactions were take into accounts for single ion anisotropy tensor calculations.[38,39] For what concerns the anisotropic exchange coupling interaction between iron ions we decided to take into account only spin dipole pair interaction. Moreover, although a few differences between DFT and point-dipole like calculation of this interaction exist,[40] we decided to use the second one which is less computational demanding. This procedure makes possible to directly map the multispin Hamiltonian $H=\sum_i \vec{s}_i \cdot \mathbf{D_i} \cdot \vec{s}_i + \sum_{i,j\neq i} \vec{s}_i \cdot \mathbf{D_{ij}} \cdot \vec{s}_j$ from DFT calculations. Thanks to the quite large J coupling constants, compared to anisotropy splitting, it was possible to take advantage of the strong exchange limit and use the Giant Spin Hamiltonian (GSH) $H=\vec{S} \cdot \mathbf{D_{S=5}} \cdot \vec{S}$, which is generally used to interpret experimental data. The multispin Hamiltonian and the GSH are related by the equation

$$\mathbf{D_S} = \sum_i d_i^S \mathbf{D_i} + \sum_{ij} d_{ij}^S \mathbf{D_{ij}} \quad (5)$$

where the projection coefficients d_i^S and d_{ij}^S were evaluated as:

$$d_i^S = \frac{\langle \alpha S||T_2(\mathbf{s}_i,\mathbf{s}_i)||\alpha S\rangle}{\langle \alpha S||T_2(\mathbf{S},\mathbf{S})||\alpha S\rangle}$$
$$d_{ij}^S = \frac{\langle \alpha S||T_2(\mathbf{s}_i,\mathbf{s}_j)||\alpha S\rangle}{\langle \alpha S||T_2(\mathbf{S},\mathbf{S})||\alpha S\rangle} \quad (6)$$

where $\langle \alpha S||\cdots||\alpha S\rangle$ stands for an irreducible matrix element of spherical tensor T_{kq}. Once the eigenket of the Heisenberg Hamiltonian (Eq. 1) $|\alpha S M_S\rangle$ have been evaluated by numerical diagonalization, d_i^S and d_{ij}^S could be calculated taking advantage of the Wigner-Eckart theorem. It is well known that DFT at the GGA level overestimates the delocalization of the charge density. This issue leads to unacceptable overestimation of antiferromagnetic interactions. For this reason, in order to study the Fe_4C_5 and the Au(111) substrate at the same time, we employed a GGA+U methodology[21] as implemented in CP2K. This procedure makes possible to correct part of the GGA deficiency without loosing high speed performances of non-hybrids functionals. In this study we used the U correction for Fe, O and Au elements of 4.1 eV, 3.0 eV and 0.60 eV, respectively. These values were taken from the works of Ninova and Malavolti *et al.*[16,17]. Spin moments for the iron ions have been calculated and reported on Table 5 of ESI for the different functionals used.

3 Results and Discussion

3.1 Bulk Structural and Magnetic Properties

One of the main issues related to the calculations of the magnetic properties at the quantum-mechanical level is the choice of the geometrical data. X-ray structures have often been considered as the best choice[41], since optimization procedures might be not accurate enough. Slight distortions of the most important geometrical parameters have significant effects on the computed magnetic properties. Indeed, the geometry optimization of molecules in the gas phase can hardly provide structures corresponding to the experimentally determined magnetic properties, which are generally measured in the solid state. Hence, in order to get a reliable bulk reference state, it is crucial to quantify the effects on the computed magnetic properties ascribed to the optimization at the DFT level and to the crystalline environment. To this purpose, the Fe_4C_5 molecule has been optimized both in vacuum (Opt-Isol model) and inside the periodic crystallographic cell (Opt-Bulk model). Optimizations have been carried out with the TPSS+D3 functional converging the electronic structures on the $S = 5$ BS state (see the Methods section for more details). The resulting Root Mean Square Deviation (RMSD) of the the Opt-Bulk model with respect to the X-ray structure is 0.10 Å. The larger contribution to the RMSD value comes from the C_5 aliphatic chains, which, however, are not well resolved in experiment. Instead, the RMSD of the iron and oxygen atoms of the magnetic core is only 0.03 Å. For the Opt-Isol model

Journal of Materials Chemistry C Accepted Manuscript

the global RMSD amounts to 0.12 Å, while it is reduced to 0.04 Å considering only the core of the molecule. Considering the strong dependence of the magnetic properties on structural parameters, particular attention has been devoted to check the agreement between experimental and computed Fe_cOFe_p and γ-pitch angles of the propeller structure.

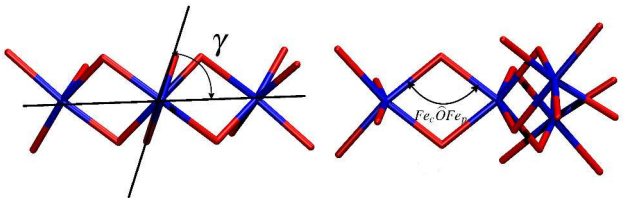

Fig. 2 (a): the γ-pitch angle; (b): the FeOFe angle. Color code as in Fig. 1.

The latter is defined as the dihedral angle between the irons' plane and the plane $Fe_cO_2Fe_p$ defining the blades of the propeller structure, see Fig. 2a. Previous studies on magneto-structural correlation [15,42] evidenced that the isotropic exchange coupling between central and peripheral irons and the axial anisotropy intensity, strongly depends on the Fe_cOFe_p and the γ-pitch angles, respectively. The mean value of the Fe_cOFe_p angle for the Opt-Isol and the Opt-Bulk models deviates from the corresponding X-ray values of 1.5% and 0.9%, respectively. The average γ-pitch angle deviates of about 1.5% for both Opt models. To verify the effect of these deviations on the magnetic properties, the isotropic exchange coupling and the anisotropy tensors have been evaluated for the Opt-Bulk and Opt-Isol models (see Tables 1 and 2). We employ the same successful approach used to calculate these properties for the X-ray structures of a Fe_4 family, as reported in our previous paper [15]. The isotropic exchange coupling constants are obtained at both PBE0 and PBE+U level of theory. The PBE+U results show a slight overestimation of the antiferromagnetic contributions comparing to the PBE0 ones(see Table 1). The difference between PBE+U and PBE0 can be ascribed to the fact that the used Hubbard U parameters for Fe and O were fitted at the DFT rev-PBE level. [16] Nevertheless, our results show the good transferability of the U parameters within the Fe_4 class of SMMs.

The effective C_2 symmetry of the molecule is correctly retained only in the Opt-Bulk model, which turns out to be less antiferromagnetic than the corresponding X-ray structure (see Table 1). A further decrease of J has been obtained for the Opt-Isol model. The same trend has been observed for both the PBE0 and PBE+U approaches. This confirms the strong dependence of the magnetic properties on small geometrical

Table 1 Fe_4C_5 Crystal Magnetic Properties

	Functional	X-ray[a]	Opt-Bulk[a]	Opt-Isol[a]	Exp
J_{12} (cm^{-1})	PBE0	17.4	13.2	9.8	-
	PBE+U	21.5	16.2	13.9	
J_{13} (cm^{-1})	PBE0	15.3	8.1	5.0	-
	PBE+U	19.2	11.7	8.8	
J_{14} (cm^{-1})	PBE0	15.3	7.8	8.6	-
	PBE+U	19.1	11.4	12.5	
J_1 (cm^{-1})[b]	PBE0	16.4	9.7	7.8	16.74
	PBE+U	19.9	13.4	11.8	
J_2 (cm^{-1})	PBE0	0.2	0.1	0.1	0.5
	PBE+U	0.4	0.2	0.2	

[a] Selected molecule inside the Fe_4C_5 crystal;
[b] J_{12}, J_{13} and J_{14} average value.

variations, thus emphasizing the importance of accurate reference structures. Previous studies on iron dimers and Fe_4 molecules [15,43] suggest that the FeOFe angle variations have the largest effect on J_1. Instead, in the Opt-Bulk model a large decrease of J_1 seems to be induced by a slightly changed Fe_cOFe_p angle. Most of the structural differences between X-ray and Opt-Bulk come from the rotation of the two tripodal ligands along the pseudo C_3 symmetry axis. This rotation occurs without changing the position of the oxygen atoms. It rather modifies the out-of-plane angle of the alchoxy-nearest carbon with respect to the Fe_c-O-Fe_p plane. Test calculations over an iron dimer model support the hypothesis that also this degree of freedom could affect the isotropic exchange interaction between μ-alchoxy bridged iron clusters (see ESI for further explanations).

Table 2 Fe_4C_5 Crystal Magnetic Properties

	Functional	X-ray[a]	Opt-Bulk[a]	Opt-Isol[a]	Exp
D_1 (cm^{-1})	PBE	-1.105	-1.050	-1.046	-
E/D_1		0.03	0.01	0.11	
D_2 (cm^{-1})	PBE	0.818	0.639	0.650	-
E/D_2		0.16	0.20	0.21	
D_3 (cm^{-1})	PBE	0.731	0.619	0.540	-
E/D_3		0.17	0.18	0.22	
D_4 (cm^{-1})	PBE	0.731	0.628	0.591	-
E/D_4		0.17	0.18	0.20	
$D_{S=5}$ (cm^{-1})	PBE	-0.475	-0.426	-0.425	-0.451
$E/D_{S=5}$	PBE	0.02	0.03	0.06	0.01

[a] Selected molecule inside the Fe_4C_5 crystal;

For what concerns the axial anisotropy parameter, D, the symmetry properties are correctly retained in the Opt-Bulk model and this seems to be sufficient to get a good agreement

Journal of Materials Chemistry C Accepted Manuscript

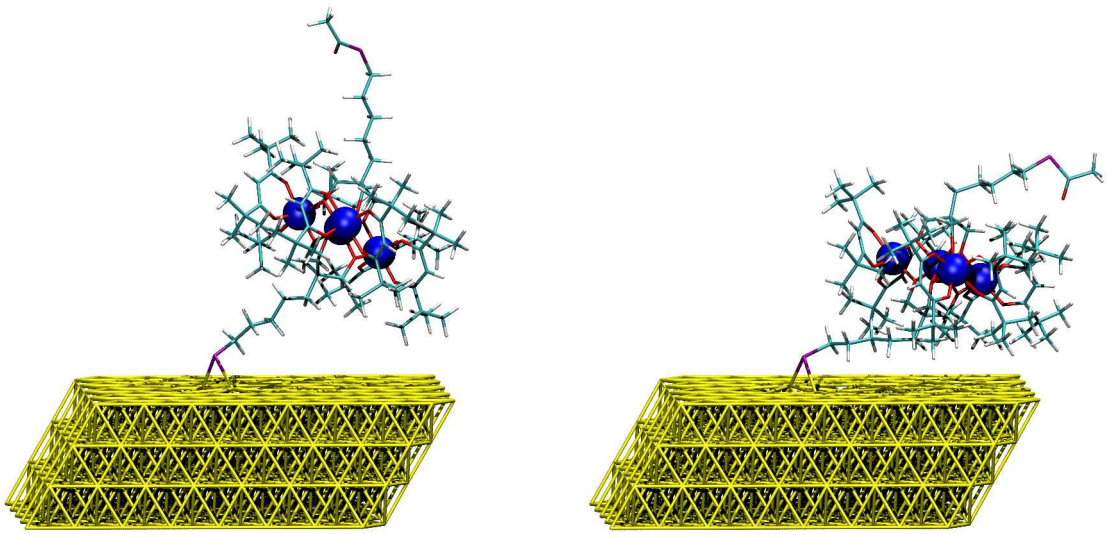

Fig. 3 On the left the Fe_4C_5@Au(111) starting configuration used for the AIMD simulation (GeoUp). On the right one snapshot extracted from the trajectory after thermalization (GeoDown). Color code as in Fig. 1. Yellow is used for the gold atoms.

with experiment. Apparently, the structural changes generated by the optimization have a marginal effect on this quantity. These results shed light on the importance of studying the condensed phase to reproduce the experimental properties.

As a summary, the Opt-Bulk model is preferable to reproduce both geometrical and magnetic features of Fe_4C_5 and thus it is selected as reference model.

3.2 Fe_4C_5@Au(111) Molecular Dynamics and Structures Relaxation

The DFT-optimized structure published by Mannini *et al.*[6] was obtained with the bare TPSS functional as were not available vdW correction methods at the time. This structure has been optimized with the computational set up explained in the Methods section but the inclusion of D3 corrections does not significantly change the Fe_4C_5@Au(111) structure. This geometry (GeoUp model, Fig. 3 left panel), already found by Mannini *et al.*[6] is the starting configuration for the AIMD simulations. The initial thermalization run at 200 K ($\sim$ 3 ps) has produced important structural changes and a stabilization of about 77 kcal mol^{-1}. The new relaxed geometry (GeoDown model, see Fig. 3 right panel) is characterized by the collapse of the aliphatic C_5 chain on the gold surface, so that the organic scaffold of the magnetic irons core is significantly closer to both the surface and the aliphatic chain itself. Moreover, the angle θ, defined as the angle between the normal to the plane of the four irons and the surface normal, is significantly smaller (see Fig. 3). θ is related to the easy-axis direction of the spin ground state anisotropy. As a consequence of this rearrangement, also the magnetic core undergoes a strong deformation, with the loss of the C_2 symmetry axis along the Fe_1-Fe_2 bond.

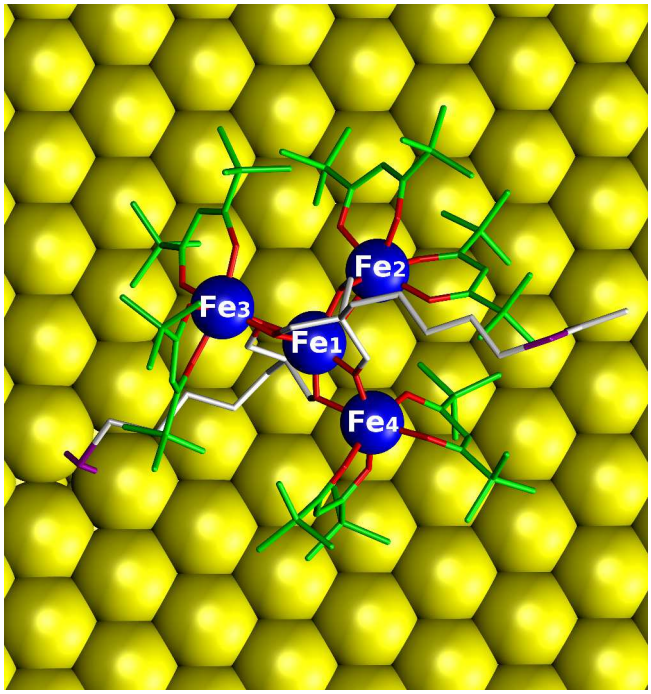

Fig. 4 Top view of an AIMD snapshot. Color code as in Fig. 3 but for the C_5 aliphatic chains' carbon atoms colored in white.

In order to sample the configurational landscape of Fe_4C_5@Au(111) at finite temperature, we started eight independent AIMD simulations from the minimum structure found after the thermalization. In order to generate independent tra-

Journal of Materials Chemistry C Accepted Manuscript

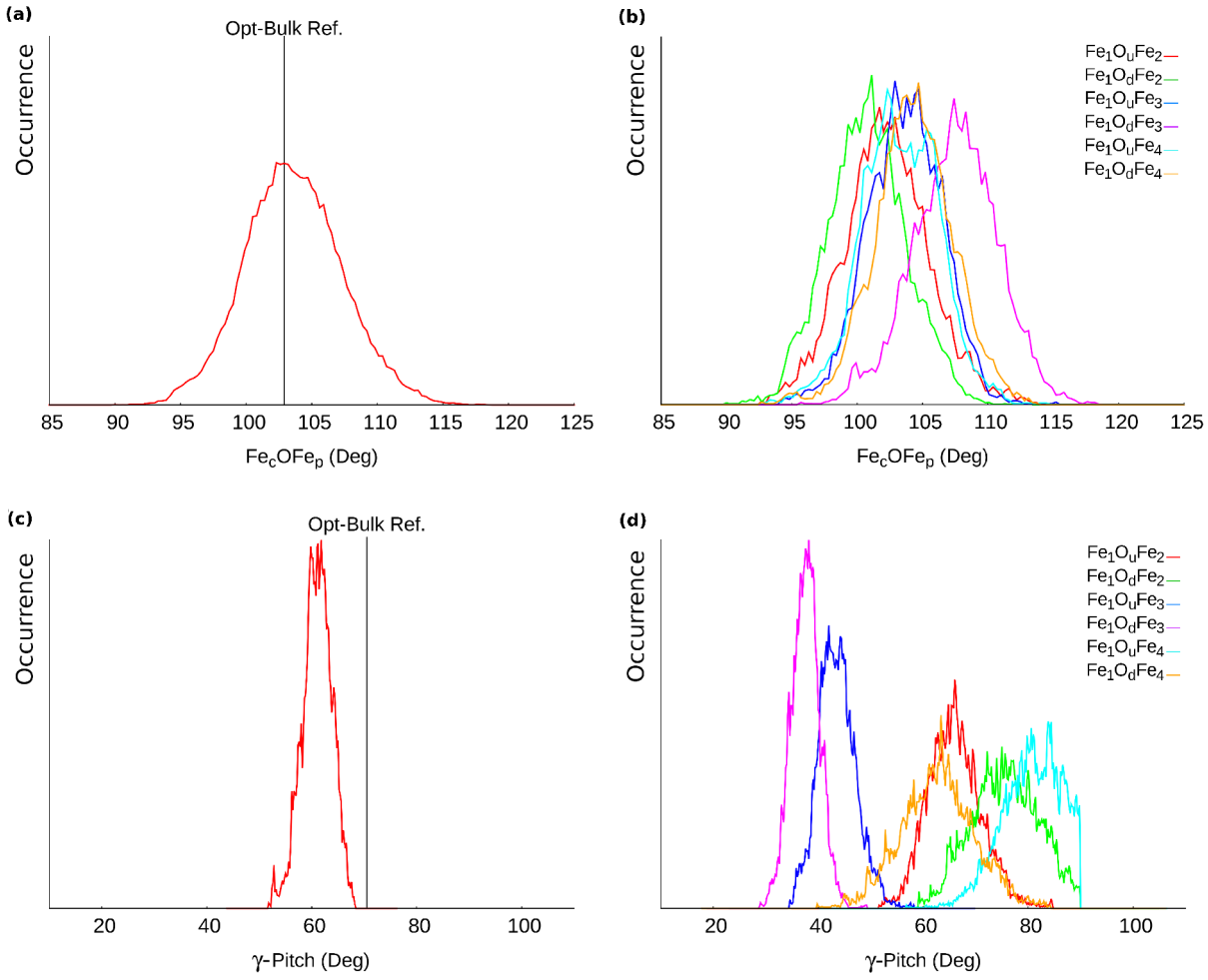

Fig. 5 (a): Molecular average FeOFe angle's normalized distribution. (b): Single FeOFe angle's normalized distributions. (c): Molecular average γ-pitch angle's normalized distribution. (d): Single γ-pitch angle's normalized distributions.

jectories spanning the accessible phase space, the velocities have been differently initialized (details in Methods). Each independent run consists of a thermalization part at 200 K, followed by a sampling part at equilibrium. The sum of all eight sampling times amounts to 20 ps, which can be used for the analysis of the equilibrium properties of Fe_4C_5@Au(111) at 200 K. We observe that all trajectories span the same region of the configurational space, which suggests that a stable minimum is already reached during the thermalization. The C_5 aliphatic chain remains in close contact with one dpm ligand of Fe_3, while the other dpm are free to lay in contact with the surface (see Fig. 4). As a consequence, the molecule turns out to be tilted with respect to the surface normal and the symmetry elements of the Fe_4C_5 magnetic core are completely removed.

The statistical distributions of Fe_cOFe_p, γ-pitch, and θ angles, reported in Fig. 5 and Fig. 6, provide an interesting overview on the observed distortions. The mean value of the Fe_cOFe_p angle, averaged over the three Fe_c-Fe_p couples inside the molecule, is 103.8° (Fig. 5a). This value is only slightly larger than the value characterizing the X-ray geometry: 102.6°. Splitting the average into the single angle contributions, both for the oxygen above (O_u) and below (O_d) the iron ions' plane, as showed in Fig. 5b, it is noticed that the $Fe_1O_dFe_3$ distribution is shifted with respect to the others. On the other hand, the single γ-pitch angles fluctuate around quite different mean values, while the molecular average is strongly peaked at 61.1° (Fig. 5c *vs* Fig. 5d). In both cases, the larger deviation from the molecular average value is observed for the Fe_3 ion's properties. Such different behavior can be ascribed to the fact that this ion is the one in direct contact with the C_5 chain.

Even though Fe_4C_5@Au(111)'s local magnetic centers undergo severe geometrical distortions upon grafting, the differences are partially averaged at the molecular level. Fig. 6 shows that θ explores angles between 10° and 25° with a

Journal of Materials Chemistry C Accepted Manuscript

Table 3 AIMD Walkers Final Energies

	GeoUp	GeoDown	Walker1	Walker2	Walker3	Walker4	Walker5	Walker6	Walker7	Walker8	Avg.[a]
E (Kcal mol^{-1})	0.0[f]	-76.95	-83.43	-79.02	-79.09	-79.97	-81.54	-81.73	-81.16	-79.40	-80.67
RMSD[b]	0.64	0.00[f]	0.16	0.25	0.38	0.20	0.21	0.20	0.28	0.34	0.25
Fe_cOFe_p[c]	102.37°	102.94°	103.15°	103.54°	102.95°	103.65°	104.88°	104.23°	105.23°	104.07°	103.73
θ[e]	29.0°	14.7°	18.5°	18.0°	16.5°	16.9°	16.3°	13.9°	14.3°	17.5°	16.5°
γ-pitch[d]	67.3°	71.5°	71.1°	71.2°	68.2°	70.6°	72.7°	69.1°	70.8°	78.0°	71.4°

[a] This averaged value is calculated over the eight final AIMD structure only;
[b] Evaluated considering irons and oxygens from magnetic core region only;
[c] Averaged over the molecule, Exp. Value 102.89°;
[d] Averaged over the molecule, Exp. Value 70.45°;
[e] Estimated upper limit value by Mannini *et al.*[6] 35°;
[f] Reference value.

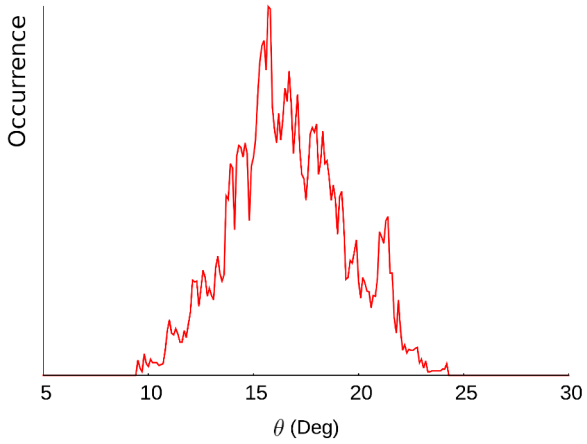

Fig. 6 The angle between the irons' plane normal and the surface's normal.

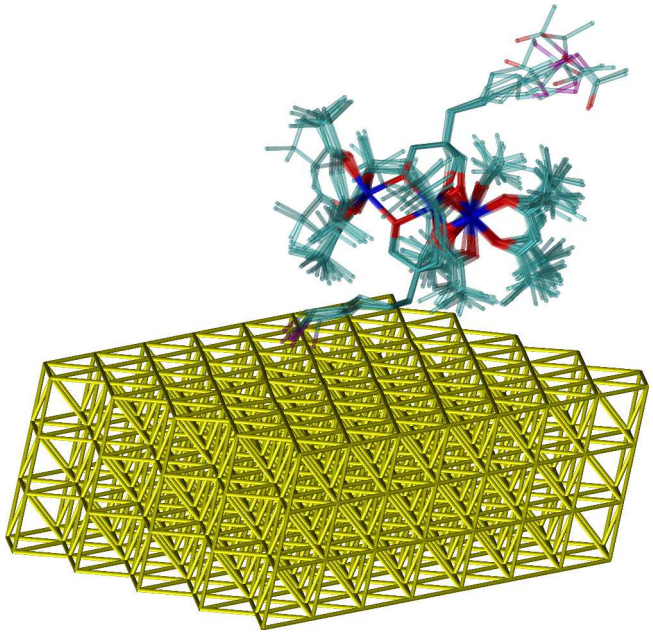

Fig. 7 Overlapped structure of all the Fe_4C_5 Walkers. Walkers' geometries have been translated over the Au(111) slab minimizing the displacement between equivalent iron ions. Color code as in Fig. 3.

mean value of 16.7°. This means that the magnetization easy-axis does not sample all the directions inside a cone, as expected.[6] Instead, it moves inside an hollow cone, avoiding the structures strictly perpendicular to the surface. The observed behavior is due to the presence of the C_5 carbon chain which remains under the organic scaffold of the Fe_4 core, thus imposing the tilt. The not innocent influence of the functionalization group of the tripod ligand on the final grafted geometry is even more evident. Indeed, if a flexible aliphatic chain can ensure a lower angle θ, it can also induce larger geometrical perturbations at the magnetic core level, which in turn might alter the Fe_4C_5 magnetic properties. SMMs magnetism becomes experimentally evident only at temperature of a few K, while AIMD generates a structural sampling at 200 K.

In principle, starting from the sampled configurations, an estimate of the magnetic properties could be extrapolated from structural magneto-correlations. However, it is preferable to get rid of the entropic contributions, *i.e.* to derive from the FES exploration the corresponding equilibrium structures on the PES. Even though on the FES the system has remained in one single basin of attraction, we found that the underlying PES is topographically corrugated, *i.e.* is characterized by several local minima. The structural features distinguishing among these minima determine fluctuations of the magnetic properties that might become important for the understanding of the experimentally observed behaviour. In order to identify possible different minima on the PES, we applied simulated

Journal of Materials Chemistry C Accepted Manuscript

Table 4 Isotropic Magnetic Properties - Fe_4C_5@Au(111) Models

	Functional	Walker1	Walker2	Walker3	Walker4	Walker5	Walker6	Walker7	Walker8	Avg
J_{12}	PBE+U	20.8	16.7	17.3	11.7	13.3	20.1	15.1	16.6	16.5
J_{13}	PBE+U	26.2	17.4	24.3	29.1	31.1	33.1	43.9	39.6	30.6
J_{14}	PBE+U	20.2	26.4	28.7	27.7	25.3	29.9	33.1	17.8	26.1
J_1[a]	PBE+U	22.4	20.2	23.4	22.8	23.3	27.7	30.7	23.8	24.3
J_2	PBE+U	0.2	-0.3	-0.5	0.3	0.7	1.1	1.2	0.7	0.4

All reported values are in cm^{-1}.
[a] J_{12}, J_{13} and J_{14} average value.

Table 5 Isotropic Magnetic Properties - Fe_4C_5@Au(111) Models

	Functional	Walker1	Walker2	Walker3	Walker4	Walker5	Walker6	Walker7	Walker8	Avg
J_{12}	PBE0	17.5	13.0	11.0	7.8	11.0	14.8	12.0	13.7	12.6
	PBE+U	21.5	17.8	16.7	11.6	14.0	19.5	15.8	17.0	16.7
J_{13}	PBE0	23.4	16.7	19.0	26.5	29.4	29.8	39.0	32.9	27.1
	PBE+U	27.9	21.0	25.1	31.6	34.2	35.2	46.8	38.3	32.5
J_{14}	PBE0	16.3	22.1	24.0	24.6	23.4	29.4	29.7	15.2	23.1
	PBE+U	20.9	25.1	30.2	29.6	27.6	35.0	33.7	17.7	27.5
J_1[a]	PBE0	19.1	17.4	18.0	19.6	21.3	24.7	26.9	20.6	21.0
	PBE+U	23.4	21.3	24.0	24.3	24.0	29.9	32.1	24.4	25.4
J_2	PBE0	0.2	0.2	0.1	0.2	0.1	0.1	0.2	0.2	0.2
	PBE+U	0.0	-0.1	1.8	0.4	0.3	0.4	0.2	0.3	0.4

All reported values are in cm^{-1}.
[a] J_{12}, J_{13} and J_{14} average value.

thermal annealing (from 200 K to a few K) to the final configuration of each of the eight generated trajectories. Each annealing has been followed by a structure optimization. Energies, RMSD and selected geometrical parameters for the eight optimized geometries (Walker1-8 from now on) are summarized in Table 3. All the structures are in a range of few kcal mol^{-1} in energy. With respect to the GeoDown model, they are approximately 4 kcal mol^{-1} more stable. RMSD (only for iron and oxygen atoms) values and Fe_cOFe_p and θ angles are close to the averages of the corresponding distributions as obtained along the AIMD sampling, and differ substantially from those calculated for the GeoUp model. The most evident structural parameter that distinguishes the eight Walkers is the position of the dangling C_5-SAc aliphatic chain, as illustrated by the overlap of eight sets of coordinates in Fig. 7. Small, but significant from the magnetic point of view, deviations in the core region are also observed, which point to a distribution of the values of certain magnetic properties, even though these structures belong to the same minimum on the FES.

3.3 Magnetic Properties Analysis

As discussed above, in order to employ a consistent electronic structure method to compare magnetic properties of Bulk-Opt model and the Fe_4C_5@Au(111), we adopt the PBE+U approach to evaluate isotropic exchange coupling constants. As for Bulk-Opt, Fe_4C_5@Au(111) retains antiferromagnetic exchange interaction between iron ions and the $S = 5$ ground state multiplicity. The average values of the Js reported in the last column of Table 4 reveal a stronger antiferromagnetic character for Fe_4C_5@Au(111) than for Opt-Bulk. In particular, J_1 increases of about 11 cm^{-1} and J_2 of about 0.2 cm^{-1}. The bulk pseudo C_3 symmetry is here lost and the individual J_{12}, J_{13} and J_{14} values are quite different one from each other. According to the structural analysis made in the last section, these J_{1x} differences could be attributed to the removal of any symmetry elements for the four iron ions upon grafting. The J_1 values are all larger than the bulk reference, as expected from the increase of the Fe_cOFe_p angles. It is interesting to note that the standard deviations for the two exchange coupling parameters are 3.0 cm^{-1} and 0.6 cm^{-1}, respectively. This means that the energy separation from the first excited state, $S = 4$, can range from 46 cm^{-1} to 70 cm^{-1}. The estimate for the Opt-Bulk model is significantly lower, 32 cm^{-1}, once more strongly supporting the not innocent role of the Au(111) surface. These results pose a question on the nature of the effects induced by the grafting process. In order to

Journal of Materials Chemistry C Accepted Manuscript

Table 6 Anisotropic Magnetic Properties - Fe_4C_5@Au(111) Models

	Functional	Walker1	Walker2	Walker3	Walker4	Walker5	Walker6	Walker7	Walker8	Avg
D_1	PBE	1.555	-1.138	-1.058	-1.177	-1.106	-1.105	-1.107	-1.167	-0.789
E/D_1		0.23	0.12	0.08	0.26	0.09	0.23	0.18	0.18	0.17
D_2	PBE	0.651	0.557	0.573	0.614	0.480	0.508	0.529	0.610	0.565
E/D_2		0.13	0.16	0.13	0.13	0.15	0.16	0.13	0.15	0.14
D_3	PBE	-0.375	0.536	-0.407	-0.390	-0.447	-0.362	-0.434	-0.465	-0.293
E/D_3		0.21	0.25	0.20	0.18	0.30	0.14	0.20	0.26	0.22
D_4	PBE	0.461	0.488	0.515	0.591	0.634	0.410	-0.384	0.747	0.433
E/D_4		0.24	0.23	0.21	0.17	0.14	0.23	0.32	0.19	0.22
$D_{S=5}$	PBE	-0.390	-0.403	-0.583	-0.376	-0.378	-0.343	-0.343	-0.409	-0.403
$E/D_{S=5}$	PBE	0.12	0.02	0.19	0.05	0.04	0.07	0.15	0.08	0.09
ζ		18.6°	14.2°	36.7°	15.1°	14.7°	12.2°	13.9°	15.3°	17.6°

All reported D and E/D values are in cm^{-1}.

separately address steric effects and electronic contributions of the gold surface, we removed the gold slab and computed the magnetic properties molecule keeping the same coordinates, Fe_4C_5@Au(111) model. In this case the Ac· group has been reintroduced at the S radical site, in order to avoid spurious spin contributions. Indeed, in the grafted scenario, at this site a strong Au-S bond is present. For a check on the reliability of the DFT+U correction for geometries different than the equilibrium one, the Js of the Fe_4C_5@Au(111) model have been also computed at the PBE0 level. Confirming the trend observed for the Bulk and Isolated models (see Table 1), the PBE0 values in Table 5 are systematically lower than the PBE+U ones. Otherwise, the two series of calculations over the eight walkers show the same type of fluctuations, validating the reliability of the PBE+U approach. The exchange interaction between iron ions is always antiferromagnetic and the ground state multiplicity is still $S = 5$. The comparison between J values in Tables 4 and 5 reveals that the explicit presence of the metallic substrate induces an homogeneously reduction of the J_1 values of about 1 cm^{-1}.

These data clearly show that structural rearrangements induced by the grafting process are mostly responsible for the evolution of the magnetic properties of Fe_4C_5 and the electronic effects induced by the presence of the metallic slab can be considered negligible.

Also the anisotropy parameters have been calculated for the Fe_4C_5@Au(111) system. Given the negligible effect of the Au(111) explicit presence, these parameters are expected to properly approximate the Fe_4C_5@Au(111) values. From the study of the anisotropic part of the spin Hamiltonian (reported in Table 6), we observe the significant increase in the rhombicity of the single ion anisotropy tensor for the central iron ion, with respect to the bulk calculated values. The local distortions of the octahedral environment around Fe_c are responsible for this behavior. Except for Walker1, the easy axis kind of anisotropy is retained. While no big differences with respect to the crystalline system are recorded for Fe_2 and Fe_4, the magnetic behavior of Fe_3 is modified. The dpm ligands of Fe_3 are always found to lie above the C_5 aliphatic chain. This causes the change in sign of its axial anisotropy parameter in all cases, except for Walker2, leading to an easy-axis anisotropy, in contrast with the easy plane anisotropy observed for the Opt-Bulk model. To be stressed that in spite of all these not negligeble modifications, the orientation of the single ion tensors resemble the bulk one. The easy-axis of both the central iron and the peripheral ions are almost parallel to the irons plane normal, *e.g.* the mean inclination angle of the Fe_3 easy-axis with respect to the normal is $4.8° \pm 3.7°$. The global molecular anisotropy, evaluated for the $S = 5$ ground states in the GSH approximation, is an easy-axis anisotropy and, for all the adsorbed molecules except for Walker3, its value is diminished of about the 11%, with respect to the Bulk-Opt model. The easy-axis orientation, with respect to the irons' plane normal, is retained: the easy-axis direction deviates from the peripherals irons' plane normal of about 4°. Moreover, the easy-axis direction inclination (ζ) with respect to the surface normal, evaluated from the $\mathbf{D}_{S=5}$ tensor, well matches with the angle θ for all the Walkers, except for Walker3. For Walker1, Walker3 and Walker7 we also observe the increase of the rhombicity term with respect to the Opt-Bulk model. The significant increase in the rhombic anisotropy induced by the interaction with the surface well compares with experimental observation of an increased tunnelling relaxation efficiency. Indeed, the simulation of the hysteresis loops detected by XMCD experiments by Mannini *et al.*[6] requested an increases of the E/D ratio up to 0.1 as well as the inclusion of higher order terms in the spin Hamiltonian. It should however be considered that in that case the formation of a densely packed monolayer of grafted molecules could partially limit the interaction of the aliphatic chain with the surface, reduc-

Journal of Materials Chemistry C Accepted Manuscript

ing the deformation of the magnetic core.

4 Conclusions and Future Perspectives

In this work we present a computational study of the Fe_4C_5 SMM adsorbed on Au(111). We propose a new computational protocol, which is able to predict the evolution of both structural and magnetic properties going from the bulk to the adsorbed scenario. We emphasize the importance of the AIMD approach to properly take into account the distribution of accessible configurations and to reveal, after annealing, the roughness of the PES. Selected geometrical parameter, crucial for the SMM magnetism, have been monitored both at finite and zero temperature and considerable modifications, with respect to the bulk reference values, have been observed. The relevant conclusion is that the retention of the S = 5 as ground state in the transition from bulk to @Au(111) is not due to the rigidity of the Fe_4 core but on accidental balanced structural distortions of it. In particular the not innocent influence of the C_5 aliphatic carbon linker, on the final adsorbed geometry, have been discussed. Indeed, if a long spacer chain can ensure a facilitate grafting procedure, it can also induce larger geometrical perturbations at the magnetic core level risking to alter the Fe_4C_5 magnetic structure. For this reason, a more rigid functionalization group, with less degrees of freedom, could reduce such a risk.

The combination of AIMD sampling, annealing procedures, and magnetic properties calculations at the DFT level of theory allowed to shed light on the effects of structural rearrangements and of the surface coupling on grafted SMMs. The fact that the electronic coupling with gold has a marginal role is in contrast to what observed for metal phtalocyanines and metal porphirins, where, instead, the metal is in direct contact with the surface and the metal's magnetic orbitals could strongly hybridize with surface's states.[44–46].

From a perspective point of view, this work paves the ground for further experimental and computational studies. Indeed, the confirmation of the importance of the aliphatic carbon spacer and the demonstration of the overcoming importance of structural rearrangements over electronic effects induced by the surface on magnetism show how could be important a chemical tailoring strategy, of the organic scaffold of SMMs, in order to modulate and control the SMMs' magnetic properties on surface. In this context, further studies on different linkers and on effects of molecular packing on the surface become of primary importance.

5 Acknowledgement

We thank the European Research Council for funding through the Advanced Grant MolNanoMaS (no. 267746), Italian MIUR for support through FIRB project *Nanomagneti molecolari su superfici metalliche e magnetiche per applicazioni nella spintronica molecolare* (RBAP117RWN), and the CINECA award under the PRACE ("DySMoMAu" 5th PRACE call n. 2012061051) initiative, for the availability of high performance computing resources and support.

References

1 S. Loth, K. von Bergmann, M. Ternes, A. F. Otte, C. P. Lutz and A. J. Heinrich, *Nat. Phys.*, 2010, **6**, 340–344.
2 S. Loth, S. Baumann, C. P. Lutz, D. M. Eigler and A. J. Heinrich, *Science*, 2012, **335**, 196–199.
3 L. Bogani and W. Wernsdorfer, *Nat. Mater.*, 2008, **7**, 179–186.
4 D. Gatteschi, L. Bogani, A. Cornia, M. Mannini, L. Sorace and R. Sessoli, *Solid State Sci.*, 2008, **10**, 1701–1709.
5 R. Sessoli, D. Gatteschi, A. Caneschi and M. A. Novak, *Nature*, 1993, **365**, 141–143.
6 M. Mannini, F. Pineider, C. Danieli, F. Totti, L. Sorace, P. Sainctavit, M.-A. Arrio, E. Otero, L. Joly, J. C. Cezar, A. Cornia and R. Sessoli, *Nature*, 2010, **468**, 417–421.
7 M. Mannini, F. Pineider, P. Sainctavit, C. Danieli, E. Otero, C. Sciancalepore, A. M. Talarico, M.-A. Arrio, A. Cornia, D. Gatteschi and R. Sessoli, *Nat. Mater.*, 2009, **8**, 194–197.
8 A. Cornia, M. Mannini, P. Sainctavit and R. Sessoli, *Chem. Soc. Rev.*, 2011, **40**, 3076–3091.
9 F. Totti, G. Rajaraman, M. Iannuzzi and R. Sessoli, *J. Phys. Chem. C*, 2013, **117**, 7186–7190.
10 S. Barraza-Lopez, M. C. Avery and K. Park, *J. Appl. Phys.*, 2008, **103**, 07B907.
11 J. Dreiser, C. Wackerling, M. E. Ali, C. Piamonteze, F. Donati, A. Singha, K. S. Pedersen, S. Rusponi, J. Bendix, P. M. Oppeneer, T. A. Jung, H. Brune, C. M. Physics, E. Polytechnique, S. L. Source and V. Psi, *ACS Nano*, 2014, **8**, 4662–4671.
12 K. Tarafder, S. Kanungo, P. M. Oppeneer and T. Saha-Dasgupta, *Phys. Rev. Lett.*, 2012, **109**, 1–5.
13 P. Maldonado, S. Kanungo, T. Saha-Dasgupta and P. M. Oppeneer, *Phys. Rev. B*, 2013, **88**, 1–4.
14 N. Nair, J. Ribas-Arino, V. Staemmler and D. Marx, *J. Chem. Theory Comput.*, 2010, **6**, 569–575.
15 A. Lunghi and F. Totti, *J. Mater. Chem. C*, 2014, **2**, 8333–8343.
16 S. Ninova, V. Lanzilotto, L. Malavolti, L. Rigamonti, B. Cortigiani, M. Mannini, F. Totti and R. Sessoli, *J. Mater. Chem. C*, 2014, **2**, 9599–9608.
17 L. Malavolti, V. Lanzilotto, S. Ninova, L. Poggini, I. Cimatti, B. Cortigiani, L. Margheriti, D. Chiappe, E. Otero, P. Sainctavit, F. Totti, A. Cornia, M. Mannini and R. Sessoli, *Nano Lett.*, [Online early acces]. DOI: 10.1021/nl503925h. Published Online: December 9, 2014.
18 J. Otsuki, *Coord. Chemi. Rev.*, 2010, **254**, 2311–2341.
19 J. Tao, J. Perdew, V. Staroverov and G. Scuseria, *Phys. Rev. Lett.*, 2003, **91**, 146401.
20 S. Grimme, J. Antony, S. Ehrlich and H. Krieg, *J. Chem. Phys.*, 2010, **132**, 154104.
21 S. L. Dudarev, G. A. Botton, S. Y. Savrasov, C. J. Humphreys and A. P. Sutton, *Phys. Rev. B*, 1998, **57**, 1505–1509.
22 H. Häkkinen, *Nat. Chem.*, 2012, **4**, 443–455.
23 M. Jaccob, G. Rajaraman and F. Totti, *Theor. Chem. Acc.*, 2012, **131**, 1150.
24 P. Totaro, L. Poggini, A. Favre, M. Mannini, P. Sainctavit, A. Cornia, A. Magnani and R. Sessoli, *Langmuir*, 2014, **30**, 8645–9.
25 F. Pineider, M. Mannini, C. Danieli, L. Armelao, F. M. Piras, A. Magnani, A. Cornia and R. Sessoli, *J. Mater. Chem.*, 2010, **20**, 187–194.
26 G. Rajaraman, A. Caneschi, D. Gatteschi and F. Totti, *Phys. Chem. Chem. Phys.*, 2011, **13**, 3886–3895.
27 J. VandeVondele, M. Krack, F. Mohamed, M. Parrinello, T. Chassaing and J. Hutter, *Comput. Phys. Commun.*, 2005, **167**, 103–128.

Journal of Materials Chemistry C Accepted Manuscript

28 J. Hutter, M. Parrinello and G. Lippert, *Theor. Chem. Acc.*, 1999, **103**, 124–140.

29 J. Hutter, M. Iannuzzi, F. Schiffmann and J. VandeVondele, *Wiley Interdiscip. Rev.: Comput. Mol. Sci.*, 2014, **4**, 15–25.

30 J. VandeVondele and J. Hutter, *J. Chem. Phys.*, 2007, **127**, 114105.

31 C. Hartwigsen, S. Gœ decker and J. Hutter, *Phys. Rev. B*, 1998, **58**, 3641–3662.

32 M. Krack, *Theor. Chem. Acc.*, 2005, **114**, 145–152.

33 G. Bussi, D. Donadio and M. Parrinello, *J. Chem. Phys.*, 2007, **126**, 014101.

34 J. P. Perdew, M. Ernzerhof and K. Burke, *J. Chem. Phys.*, 1996, **105**, 9982.

35 M. Guidon, J. Hutter and J. VandeVondele, *J. Chem. Theory Comput.*, 2010, **6**, 2348–2364.

36 L. Noodleman, *J. Chem. Phys.*, 1981, **74**, 5737–5743.

37 A. Bencini and F. Totti, *J. Chem. Theory Comput.*, 2009, **5**, 144–154.

38 F. Neese, *J. Chem. Phys.*, 2007, **127**, 164112.

39 S. Schmitt, P. Jost and C. van Wüllen, *J. Chem. Phys.*, 2011, **134**, 194113.

40 C. Riplinger, J. P. Y. Kao, G. M. Rosen, V. Kathirvelu, G. R. Eaton, S. S. Eaton, A. Kutateladze and F. Neese, *J. Am. Chem. Soc.*, 2009, **131**, 10092–106.

41 C. Adamo, V. Barone, A. Bencini, F. Totti and I. Ciofini, *Inorg. Chem.*, 1999, **38**, 1996–2004.

42 L. Gregoli, C. Danieli, A.-L. Barra, P. Neugebauer, G. Pellegrino, G. Poneti, R. Sessoli and A. Cornia, *Chem. - Eur. J.*, 2009, **15**, 6456–6467.

43 F. Le Gall, F. Fabrizi de Biani, A. Caneschi, P. Cinelli, A. Cornia, A. C. Fabretti and D. Gatteschi, *Inorg. Chim. Acta*, 1997, **262**, 123–132.

44 Y. Y. Zhang, S. X. Du and H.-J. Gao, *Phys. Rev. B*, 2011, **84**, 125446.

45 N. Ballav, C. Wäckerlin, D. Siewert, P. M. Oppeneer and T. A. Jung, *J. Phys. Chem. Lett.*, 2013, **4**, 2303–2311.

46 C. Wäckerlin, K. Tarafder, D. Siewert, J. Girovsky, T. Hählen, C. Iacovita, A. Kleibert, F. Nolting, T. A. Jung, P. M. Oppeneer and N. Ballav, *Chem. Sci.*, 2012, **3**, 3154–3160.

Journal of Materials Chemistry C Accepted Manuscript

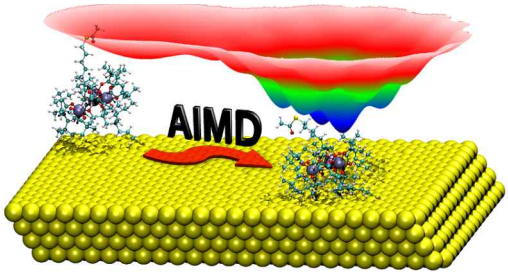

The adsorption process on gold and its consequences on the magnetic behavior of $\{Fe_4\}$ SMM has been highlighted through AIMD.

Journal of Materials Chemistry C Accepted Manuscript